Time-resolved proton polarisation (TPP) images tyrosyl radical sites in bovine liver catalase.

Oliver Zimmer, Hélène Marie Jouve, Heinrich Stuhrmann

IOP Conf. Series: Journal of Physics: Conf. Series **848** (2017) 012002 doi:10.1088/1742-6596/848/1/012002

Time-resolved proton polarisation (TPP) images tyrosyl radical sites in bovine liver catalase.

Oliver Zimmer[1], Hélène M Jouve[2], and Heinrich B Stuhrmann[2,3]

[1] Institut Laue-Langevin, F-38042 Grenoble, CEDEX 9, France.
[2] Institut de Biologie Structurale Jean-Pierre Ebel, CEA/CNRS/UJF, F-38027 Grenoble CEDEX 1, France.
[3] Helmholtz-Zentrum Geesthacht, D-21494 Geesthacht, Germany.

heinrich.stuhrmann@orange.fr

Abstract. A differentiation between dynamic polarised protons close to tyrosyl radical sites in catalase and those of the bulk is achieved by time-resolved polarised neutron scattering. Three radical sites, all of them being close to the molecular centre and the heme, appear to be equally possible. Among these is tyr-369 the radial site of which had previously been proven by EPR.

1. Introduction

At first sight, it appears that an enzyme like bovine liver catalase does not have much in common with polarized proton spin targets. The latter are used in experiments of high energy physics, whereas a redox enzyme like catalase is treated in life sciences. We will show that it is polarized neutron scattering which connects both worlds. Before entering into this complex undertaking, it seems to be appropriate to describe some aspects of both worlds, which may bear a tremendous potential of synergies in neutron scattering [1].

Let us start with polarized protons. It is widely established that abundant spin-½ nuclei, and protons in particular, in a paramagnetically doped insulator, like most hydrogenous organic materials are, reach thermal equilibrium with the lattice *via* interaction with paramagnetic impurities, e.g. unpaired electrons [2]. The theoretical foundation of this nuclear relaxation process has been formulated by Bloembergen [3] who postulated that nuclear spins *close* to paramagnetic centers are relaxed by fluctuations in the magnetic field of the paramagnetic center (direct relaxation) and that *bulk* spins are relaxed by diffusion of Zeeman energy to *close* nuclei (spin diffusion). The number of close protons in direct contact with the non-Zeeman electron-electron spin interaction reservoir (or bath) is limited by the fact that the local spin lattice relaxation rate is inversely proportional to the sixth power of the distance between the unpaired electron and the proton [2] [4]. The result is a gradient of proton polarization reflecting a proton spin diffusion barrier which separates the close protons from those of the bulk. As the local magnetic field near an unpaired electron is very large, the Larmor frequencies of the close protons differ appreciably from those of the bulk. Consequently close protons hardly contribute to the NMR signal of the bulk (Fig.1). It is this picture which provides the environment of dynamic nuclear spin polarization (DNP).

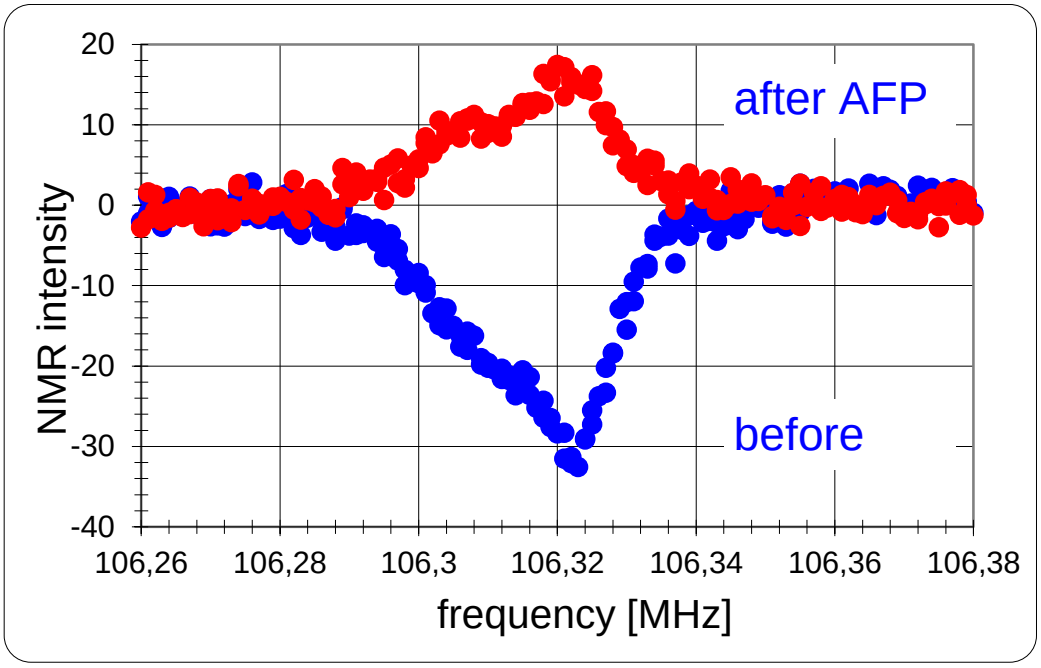

Fig. 1. The NMR intensity from tyrosyl doped catalase is due to the dynamically polarised protons of the bulk.. ● negative proton polarization with microwave irradiation at a frequency slightly above the EPR line of the tyrosyl radical, ● after adiabatic fast passage (AFP) using an rf sweep across the NMR profile. B= 2.5 T, T = 0.1K.

Dynamic nuclear spin polarization is a widely used method to polarize nuclear spins. The macroscopic aspects of DNP are well understood in the frame of the spin temperature theory [5]. The thermodynamic model of DNP assigns two heat reservoirs to various degrees of freedom of the electronic and nuclear spin system via mutual and external interactions[5] [6]. The mechanism of DNP then is described as a two-step process: the cooling of the non-Zeeman reservoir by a non-saturating microwave field at frequencies close to the electronic resonance and the subsequent transfer of entropy from the nuclear Zeeman system consisting of the close protons. Depending on the type and density of the unpaired electrons in the sample and the external conditions (temperature, applied magnetic field) DNP proceeds either by the so-called solid effect or by thermal mixing or a combination of them [5] [7]. Note that the exact type of the process is not relevant for the evaluation of the experimental data. In any case, it is assumed the magnitude of the mixing is strongly influenced by the microscopic structure of the material and in particular the nuclear spins close to the unpaired electron [8] [9]. The transfer of the polarization of the close protons to those of the bulk is controlled by the magnetic spin diffusion barrier as it has been mentioned above. Hence the polarization of the close protons is expected to be different from those of the bulk, particularly at the onset of the microwave irradiation.

Now let us turn to the radical proteins. Radicals play an important role in living cells. Radical intermediates allow enzymes to perform a wide variety of chemically challenging reactions. Catalase is a redox enzyme which converts hydrogen peroxide at an incredibly fast diffusion limited rate into water and molecular oxygen by offering peroxyacetic acid, a derivative of hydrogen peroxide with more steric hindrance, to bovine liver catalase the reaction differs in at least two points: first the response is slow, and second, after some intermediate steps one of the amino acids, a tyrosine, is converted into a tyrosyl radical. It is assumed that one and only one of the 20 tyrosines of each of the four subunits of catalase becomes a tyrosyl radical [10].

Finding the exact location of a (tyrosyl) radical is an important step in the understanding of the mechanism of an enzyme. Electron paramagnetic resonance is the method of choice for detecting a radical, and in favorable cases the site of the radical inside a protein molecule can be obtained from a detailed analysis of the EPR line [11]. A more general approach to determine the location of an unpaired electron is provided by magnetic neutron scattering. However, a radical doped protein can be considered as an extremely dilute paramagnet, with a correspondingly small magnetic amplitude.

If it comes to the size of the polarization dependent scattering length, then polarized nuclei, and certainly protons, are more rewarding targets. This has been realized forty years ago, when the dynamically polarized proton spins in a Nd^{3+} doped crystals of lanthanum magnesium nitrate were studied by polarized neutron scattering [12]. It took another ten years until dynamically polarized protons in non-crystalline targets have considerably widened the range of applications of neutron scattering [13] [14] [15]. These and later experiments of nuclear spin contrast variation (e.g. [16] [17] [18]) which profited from a high proton polarization dependent scattering amplitude, prepared the ground for a more detailed study of the build-up of proton polarization by polarized neutron scattering. The starting signal came from a problem of structural biology concerning the location of a tyrosyl radical in bovine liver catalase [10]. In an initial step, it led to a collaboration of groups of the IBS, Grenoble, of the CEN Grenoble, and of the PSI, Villigen.

2. First experiments with tyrosyl radicals of catalase.

Once it had been shown that free tyrosyl radicals in frozen solution do support DNP [1], similar studies were carried out with samples of catalase containing tyrosyl radicals. Microwave irradiation at frequencies slightly below the EPR line of tyrosyl leads to a slow increase of positive proton polarisation, far below the polarisation rate known from polarised targets used in high energy physics experiments. At T = 0.1 K a maximum proton polarisation of P = 3% was reached after several hours of microwave irradiation. Microwave irradiation at frequencies slightly above the EPR line leads to negative values of proton polarisation. At T = 0.1 K the proton polarisation reaches P = -0.98% (Fig. 2). With higher temperatures the difference ΔP between the extreme values of proton polarisation decrease. At T=0.5 K and 1.0 K we obtain ΔP = 0.6% and 0.2%, respectively. In the latter case, the proton polarisation remains positive and close to the proton polarisation at thermal equilibrium, P_e = 0.25%, encountered in a magnetic field strength B = 2.5 T, whatever direction of dynamic nuclear polarisation is used. There is hardly any change of the initial speed of proton polarisation with the temperature. The implications of this observation will be discussed below.

The method of adiabatic fast passage (AFP) is a powerful method to invert the sign of nuclear polarisation. Using a radio frequency sweep at an appropriate speed and power [19], a negative polarisation of protons in tyrosyl doped catalase is obtained within a second (Fig.1). Impressive this method is [20], it suffers from two drawbacks: first, a considerable part of the polarisation is lost, and second, the preparation preceding the jump of proton polarisation is long compared with the time of nuclear relaxation after AFP, which results in a poor use of neutron beam time. A solution to this problem is offered by frequently alternating the direction of dynamic polarisation. The build-up of a polarisation gradient then is observed after each change of the direction of DNP allowing for a high duty cycle. Another merit of this method is that it will focus on the polarisation of the close protons which are expected to image the electron spin density.

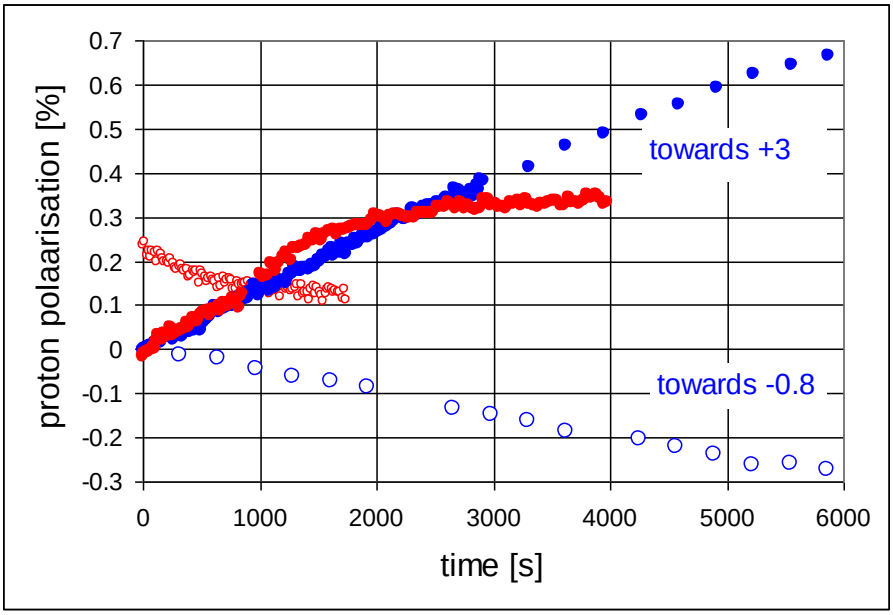

Fig. 2. The evolution of proton polarization in frozen solution of tyrosyl doped catalase with the time of microwave irradiation. ● Positive DNP at T = 0.1 K, ○ negative DNP at T = 0.1 K. ● Positive DNP at T = 1.0 K, ○ negative DNP at T = 1.0 K.

3. Experimental procedures

A detailed description of the instruments and their use for time resolved neutron scattering from dynamic polarised protons has been given earlier [21] [22]. Here we present experimental details that are necessary in order to achieve a self-contained presentation

3.1. Sample preparation

The preparation of the sample started from tetramer bovine liver catalase (BLC) in crystalline suspension (Boehringer Mannheim, Germany, lot 106828). 12 mL of the suspension were dissolved in 2 L Tris maleate buffer (50 mM, pH 7.5), purified, concentrated to 5 ml and dialyzed against 150 mL Tris maleate in D_2O. The buffer had been exchanged three times. The content of the dialysis-tube had partly precipitated, but a clear solution (0.515 mM heme) was obtained by addition of an equal volume of deuterated glycerol. Note that the BLC molecule is a tetramer enzyme with one heme as part of each of its four identical subunits. At a temperature only slightly above 0° C, to 1 mL of the clear solution of BLC 28 µL peroxyacetic acid (32% solution, Merck, diluted to 3% solution in 0.1 M Tris, and adjusted to pH 4.3) were added. The immediate formation of a tyrosyl radical can be followed by a change of the colour to deep red. After a few minutes the tyrosyl concentration reaches its maximum and the sample is frozen to liquid nitrogen temperature. From EPR measurements a tyrosyl concentration of 0.58 per heme has been determined. Samples with a lower catalase concentration were prepared in a similar way.

3.2. Neutron small-angle scattering (SANS)

The SANS measurements were performed at the D22 instrument of the Institut Laue-Langevin (ILL) Grenoble, France. We used polarized incident neutrons of wavelengths λ=4.6 Å with a wavelength spread of $\delta\lambda/\lambda = 0.1$ (FWHM). The solid sample was inserted into the NMR coil, placed in microwave cavity and mounted into a ^{4}He refrigerator, which was operated at a temperature of about 1K. A

longitudinal magnetic field of 3.5 T was provided by a superconducting split-coil solenoid. Samples could be changed and cooled down to 1K in less than half an hour.
Two IMPATT-diodes, tuned to frequencies required for positive and negative DNP, 97.2 and 97.5 GHz, respectively, could be connected to the sample cavity by a waveguide switch (total switching time 100 ms comprised of shutting within 5 ms, no microwaves for 90 ms, opening in 5 ms). Continuous wave (cw) NMR was used in parallel to monitor the proton polarisation. The direction of DNP was reversed each 5 s, and the acquisition of the polarised neutron scattering intensity was triggered synchronously in time intervals of 50 ms. Each of the 200 time frames was averaged over several thousand cycles to obtain sufficient statistical accuracy. The time dependent scattering intensity then was obtained as usual by radial averaging, and correction for polarisation dependent transmission.

4. Mathematical formalism

The evolution of the proton polarisation in space and time can be described in terms of rate equations that govern the flow of proton polarisation between the reservoirs coupled in series [22]. The reservoirs can be identified as follows: As the source of DNP, we have the electronic spin-spin interaction reservoir R0. Depending on the choice of the microwave frequency it will drive the proton polarisation towards $P = +0.98$ or $P = -0.98$, i.e. the reservoirs R0 will assume the values $P_0 = \pm 0.98$ (B=3.5 T, T = 1 K). R1 is the reservoir of the close protons that are presumably inside a spherical magnetic spin diffusion barrier with a radius of 5 Å [23]. In order to simulate a diffuse barrier, an additional reservoir, R2, of not so close protons inside a hollow sphere with an outer radius of R2 = 10 Å was assumed. R3 contains all the protons of the catalase molecule except those in R1 and R2. The protons of the deuterated solvent define R4. The protons in R3 and R4 are bulk protons, while those of R2 may be a mixture of close and bulk protons.

The build-up of proton polarisation $P_1(t)$ in R1, $P_2(t)$ in R2, $P_3(t)$ in R3 and $P_4(t)$ in R4 is governed by a set of four coupled first order differential equations:

$$\begin{aligned}
\frac{dP_1}{dt} &= \frac{W_{01}}{N_1}(P_0 - P_1) + \frac{W_{12}}{N_1}(P_2 - P_1)\\
\frac{dP_2}{dt} &= \frac{W_{12}}{N_2}(P_1 - P_2) + \frac{W_{23}}{N_2}(P_3 - P_2)\\
\frac{dP_3}{dt} &= \frac{W_{23}}{N_3}(P_2 - P_3) + \frac{W_{34}}{N_3}(P_4 - P_3)\\
\frac{dP_4}{dt} &= \frac{W_{34}}{N_4}(P_3 - P_4)
\end{aligned} \qquad (1)$$

As for the catalase molecule itself, N_i are the number of protons in Ri. N_4 is the number of solvent protons per catalase molecule. The rate constant W_{ij} are defined as probabilities of a mutual spin flip per time, e.g. the contact term W_{01} describes the flow of polarisation from R0 to R1.

The thermodynamic description of the evolution of nuclear polarisation given above has to be extended by the structural aspects which are relevant in neutron scattering. Using the expansion of the scattering amplitude as a series of spherical harmonics, we obtain the intensity of coherent small-angle scattering [1] [23]:

$$I_{coh.}(Q,t) = 2\pi^2 \sum_{l=0}^{L} \sum_{m=-l}^{m=l} \left| A_{l,m}^{(0)}(Q) + \sum_{i=1}^{3} P_i(t) B_{l,m}^{(i)}(Q) - P_4(t)\, B_{l,m}^{(4)}(Q) \right|^2 \qquad (2)$$

where $A_{l,m}(Q) = \sqrt{\frac{2}{\pi}}\, i^l \sum_n b_n\, j_l(Q r_n)\, Y_{l,m}^{*}(\theta_n, \varphi_n)$

Y and j are the spherical harmonics and spherical Bessel functions, respectively. The atomic positions are given by the polar co-ordinates r,θ,φ. The upper indices (i) > 0 refer to the reservoirs defined above. Apart from intensity of coherent scattering the experimental data of neutron scattering will contain incoherent scattering and background scattering.

$$I(Q,t) = C\,[I_{coh.}(Q,t) + I_{inc.}(t)] + I_{background}(Q,t) \qquad (3)$$

The factor C takes into account how the instrument is operated (e.g. incident neutron flux, measuring time, detector efficiency) and some properties of the sample, like concentration of the solute and the transmission of the sample.

The intensity of incoherent scattering is mainly due to the protons [24]

$$I_{inc.}(t) = \sum_{i=1}^{4} N_i \, \sigma_{incoh.}^{(i)}(t) = 8.48 \sum_{i=1}^{4} N_i \left(\frac{3}{4} - \frac{1}{2} P_i(t) - \frac{1}{4} P_i^2(t)\right) 10^{-24} \, cm^2 \qquad (4)$$

A first estimate of the background scattering intensity can be made by the measurement of the neutron scattering intensity of the empty refrigerator and the time dependent transmission of the polarised sample. There may be an additional Q- and t-dependent scattering intensity which could be due to spatially non-uniform proton polarisation, or to an intrinsic property of the instrument. These are taken into account in two ways.

1) The time-dependent background is described by a model, like the following
$$I_{background} = (c_1 P_{i<4}(t) + c_2 P_4(t))/Q^{c_3} \qquad (5)$$
2) The time dependent background scattering is substituted by that from a sample with a very low concentration of catalase.

After subtraction of $\boldsymbol{I(Q)} = 1/T_m \int_{t=0}^{T_m} I(Q,t)dt$ we obtain $Z(Q,t) = I(Q,t) - \boldsymbol{I}(Q)$. The difference between the calculated $Z_{calc.}(Q,t)$ and the measured $Z_{exp.}(Q,t)$ is minimized in an iterative procedure using as variables the scale factor C, and the rate coefficients W_{ij} and – only in case 1 – the coefficients c_1, c_2 and c_3.

$$\int_{Q=0.03}^{Q=0.09} \int_{t=0}^{t=10s} \left(Z_{exp.}(Q,t) - Z_{calc.}(Q,t)\right)^2 = Min \qquad (6)$$

The result is stabilized by including two more conditions, concerning the total scattering intensity and the variation of the NMR intensity during one cycle of DNP, respectively [18].

The equations (1) to (5) define the analysis of data from time –resolved polarised neutron scattering from protons in dynamic polarised targets. We replace this somewhat lengthy term by time-resolved proton polarisation and abbreviate it as TPP.

As the data are very noisy we use the leading members of a development as a Fourier series. $Z_{exp}(Q,t)$ then is defined as a two-dimensional array of intensities at $[m_1 \Delta Q, \; m_2 \Delta t]$ with $1 \le m_1 \le M_1$ and $1 \le m_2 \le M_2$. Omitting ΔQ and Δt we have

$$f(m_1, m_2) = \sum_{n_1=-N_1}^{N_1} \sum_{n_2=-N_2}^{N_2} F_C(n_1, n_2)\cos(z) + F_S(n_1, n_2)\sin(z) \qquad (7)$$
$$z = 2\pi \left(n_1 m_1/M_1 + n_2 m_2/M_2\right)$$

Reducing the Fourier analysis to the time axis we have

$$f(m, Q) = \sum_{n=-N}^{N} F_C(n, Q)\cos(z) + F_S(n, Q)\sin(z) \text{ with } z = 2\pi \, nm/M \qquad (8)$$

The resolution of the time-dependence will be restricted to |N|=1 throughout.

5. Results from time-resolved neutron scattering.

SANS from frozen solutions of catalase in mixtures of glycerol and D_2O as recorded by the area detector of D22 is shown in Fig. 3. The most striking feature is an unexpected important leaking out of the primary beam intensity, most likely due to an enlargement of the primary beam in the horizontal direction due the neutron spin polariser half a meter upstream the sample position. No amendment to this anomaly was made as it had been believed that these intensity peaks could well serve as measure of the time-dependent transmission of the sample.

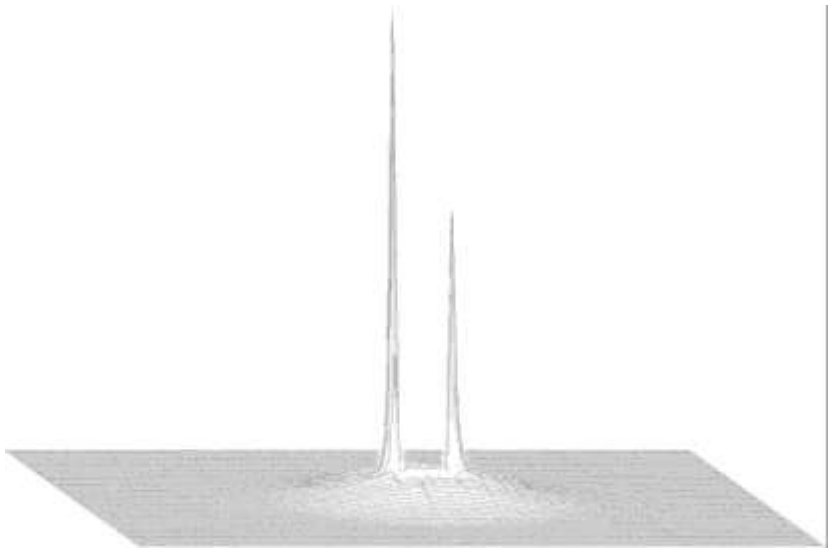

Fig. 3. Intensity of neutron scattering from catalase as recorded by the detector of D22. An important leaking out of the primary neutron beam is observed on the left and right side of the beam stop [1].

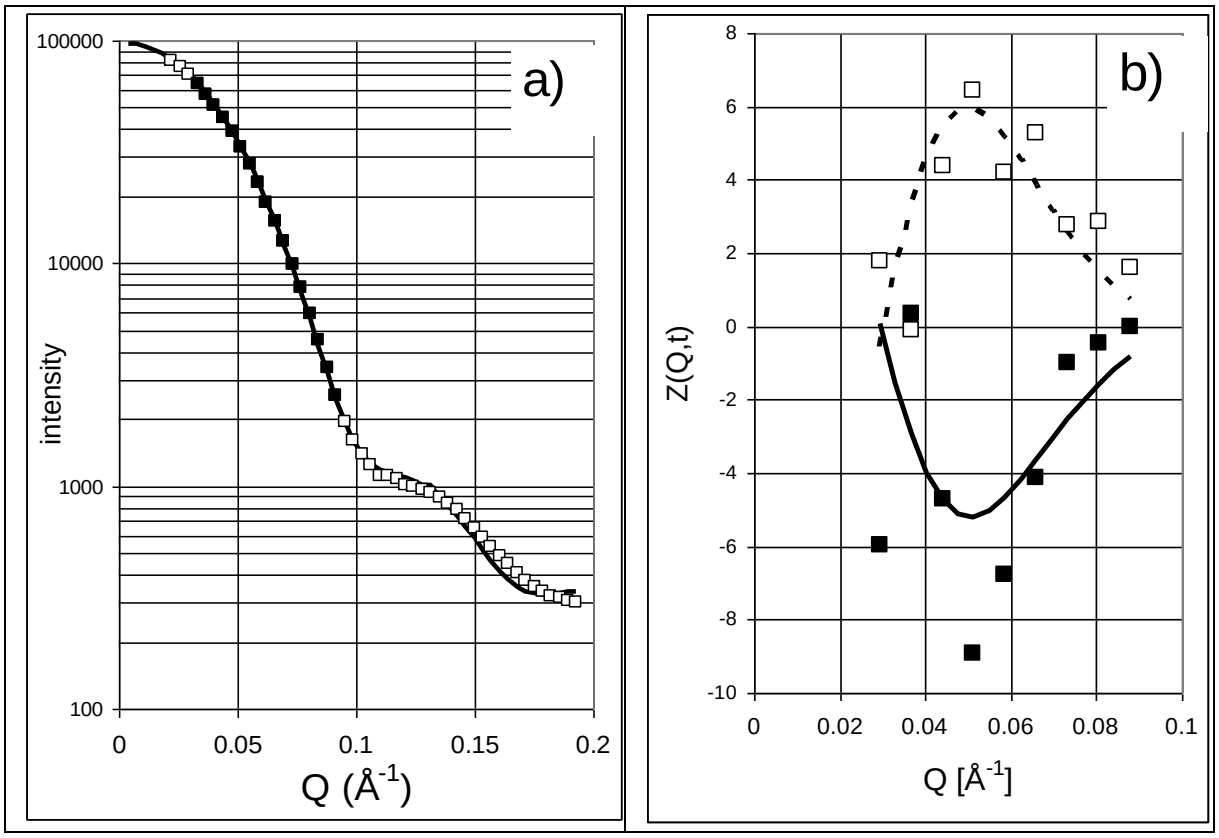

Fig. 4. SAS from catalase (a) (see text), and its time-dependent part *Z(Q,t)* at t = 2.5 s and 7.5 s in the lower and upper part of (b). Lines are experimental data after 2D Fourier analysis. At $Q = 0.05$ Å^{-1} the relative change of the intensity during one cycle of DNP amounts to 4×10^{-4} only [1].

In fact, the initial increase of the peak intensity at the onset of positive polarisation due to a decreasing transmission of the sample is compatible with the simultaneous decrease of SANS from catalase [1]. The relative change of the intensity is slightly below 1/1000 in both cases. From time resolved NMR measurement to be presented in section 6 it appears that the large change of the peak intensity cannot be reconciled with change of the transmission of the sample.

A Fourier analysis of the time dependence for each pixel contributing to the large peaks shows a regular shift of the phase defined as $\varphi = \arctan(F_S(1,Q)/F_C(1,Q)$ of 50° on passing from one to the next to the row of the area detector, i.e. the three pixels of the column on each side of the beam stop show an artefact which must be a property of the instrument rather than a physical property of the sample [1]. The question arises how to deal with this artefact and in particular how to separate it from SAS of catalase. Two approaches have been tried:

1) A 2D Fourier analysis is used with N_1=3 for the Q-axis. The background is described by (5).
2) A 1D Fourier analysis is used. SAS from catalase then is given as the difference between the intensity from a sample with a high concentration of catalase diminished by that from a sample with low concentration catalase. $F_C^{(high)}(1,Q) - F_C^{(low)}(1,Q)$ and $F_S^{(high)}(1,Q) - F_S^{(low)}(1,Q)$.

The measured intensity profile of SAS from catalase agrees with that of the obtained from the crystallographic model [25] (line in Fig. 4a). The experimental data at Q values between 0.03 and 0.09 Å^{-1} (■ in Fig. 4a) are used for a further analysis. The decrease of the time-dependent scattering $Z_{exp}(Q,t)$ at $Q < 0.05$ Å^{-1} is the signature of an instrument dependent response function mentioned above.

Using the background scattering defined by (5) and taking the radical site at tyr-369 for granted [10], $Z_{exp}(Q,t)$ in terms of the 2D Fourier analysis is reasonably well approximated by $Z_{calc.}(Q,t)$ derived from the model (Fig. 5a). There is an increasing fraction of background scattering at smaller Q (Fig. 5b).

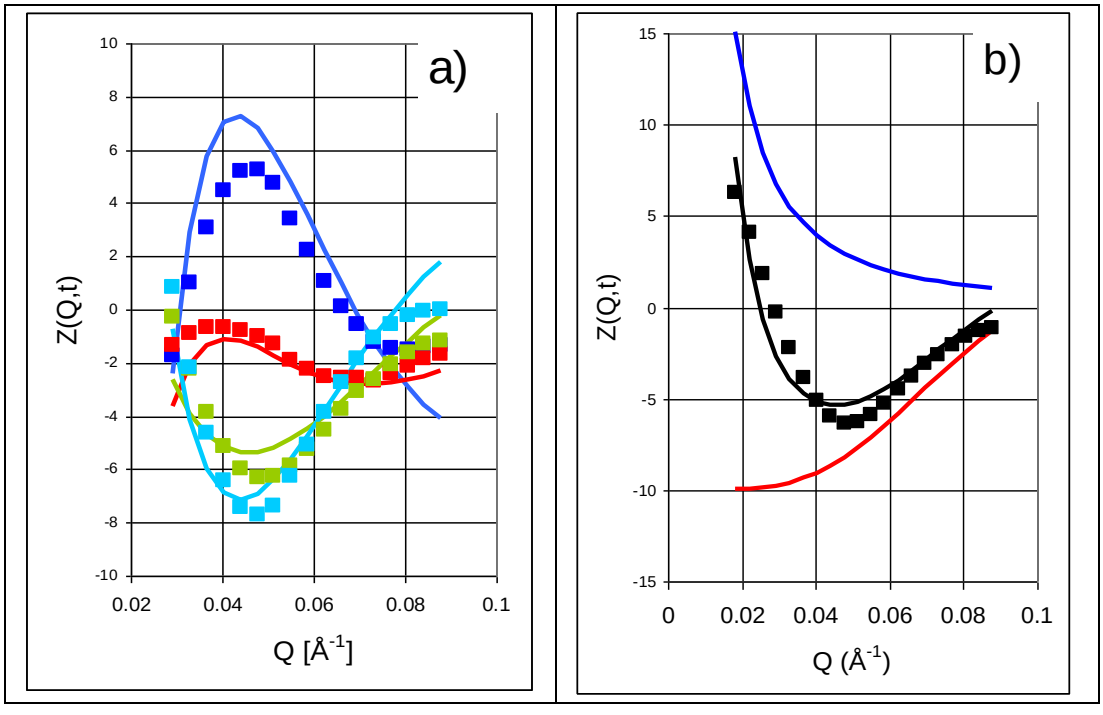

Fig. 5. Comparison of $Z_{exp}(Q,t)$ with $Z_{calc.}(Q,t)$ for various times of the cycle of DNP (a), and its decomposition into SAS from catalase and background scattering (b). a) $Z_{exp}(Q,t)$ at ■ t=0, ■ t=1.25 s, ■ t=2.5 s, ■ t=3.75 s, after 2D Fourier analysis. The corresponding $Z_{calc.}(Q,t)$ are presented as lines. b) Decomposition of $Z_{calc}(Q,t)$ (——) into SAS from catalase (——) and $I_{background}(Q,t)$ (——) at t = 2.5 s [1].

Starting from a 1D Fourier analysis as described under 2) a similarly good agreement between experimental and calculated $F_C(1,Q)$ and $F_S(1,Q)$ is obtained [1]. The scattering intensity for a sample with a low concentration of catalase appears to be an acceptable substitute for a blank sample containing no catalase at all.

An important spin-off of the fit of $Z_{calc.}(Q,t)$ to $Z_{exp}(Q,t)$ is the evolution of the proton polarisation $P_i(t)$ in each of the reservoirs Ri (Fig. 6).

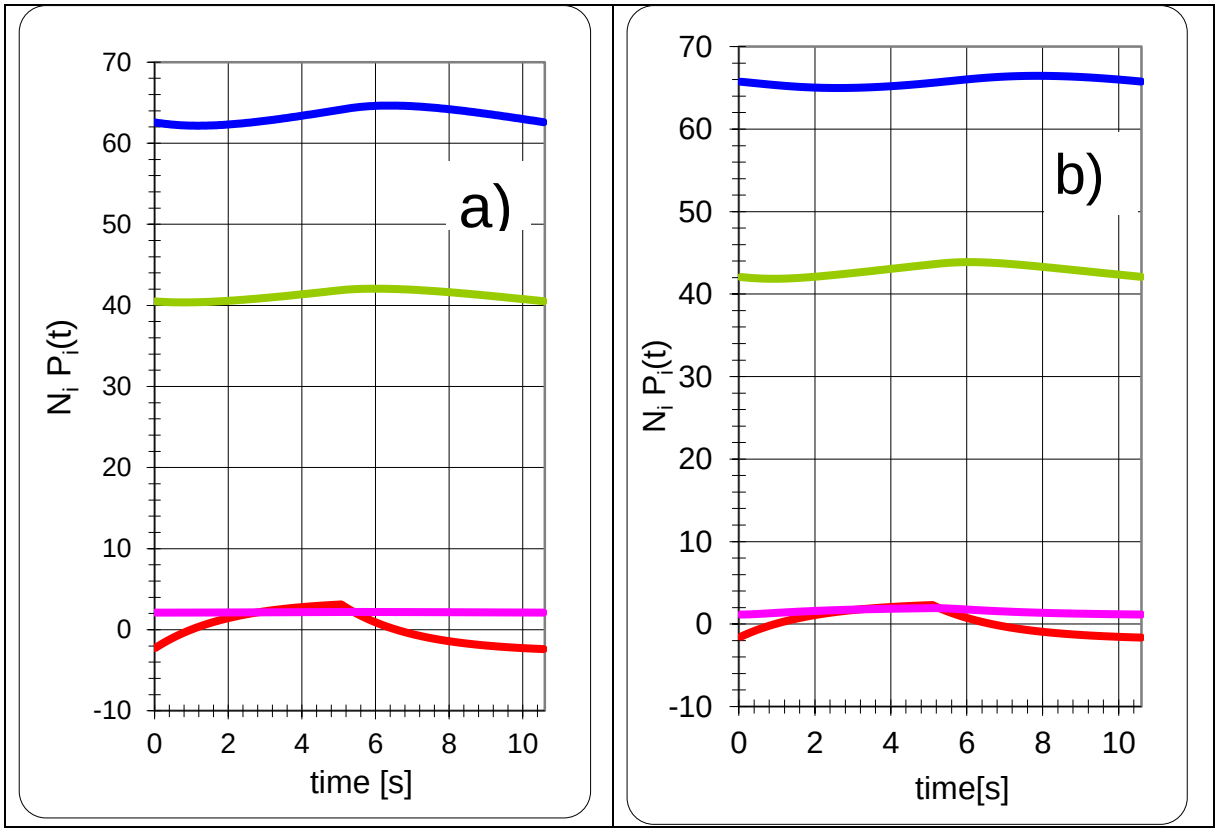

Fig. 6. The product Ni Pi(t) of the reservoirs Ri versus time. ——— i=1, ——— i=2, ——— i=3, ——— i=4. a) from a 2D Fourier series. b) from a 1D Fourier series. For the tetramer catalase molecule we have N_1 = 92(62), N_2=612(410), N_3 = 11700, N_4 = 18000. Taking into account the occupancy by tyrosyl in catalase of the 'active' catalase molecules N_1 and N_2 are reduced by a factor 0.67 (relevant to this figure).

The number of tyrosyl radicals per catalase molecules varies according to the binomial distribution $p_4(k)$ where k is the number of tyrosyls. Catalase with a single tyrosyl molecule will hardly contribute to dynamic polarisation because of the large inter-radical distance [1]. Catalase molecules with not more than a single radical will be disregarded. Moreover the occupancy of the radical sites determined by EPR is 0.58. Restricting the analysis to the 'active catalase molecules, i.e. those with more than one tyrosyl, the number of protons N_1 =92 in R1, and N_2 =612 in R2, is reduced to two third, i.e. 62 and 410 respectively (Fig.6). The number of polarized protons in excess, i.e. $N_P = N(up) - N(down)$, equals to the value of the ordinate. We are interested in the variation of polarized close protons N_P in R1 and R2, during one cycle of DNP, because these will image the electron spin density at the site of the radical. From Fig. 6a we obtains $N_P^{(1)}$ = 5.36 and $N_P^{(2)}$ = 0.1 polarised protons in R1

and R2, respectively. Taking into account the occupancy of 0.67 and sharing his value among four radical sites we obtain 5.37/0.67/4 = 2.0 polarised close protons per tyrosyl. An increase of $N_P^{(2)}$ in R2 at the expense of $N_P^{(1)}$ in R1 is obtained from data subjected to a 1D Fourier analysis.(Fig.6b). In detail we have $N_P^{(1)}$ = 3.85 and $N_P^{(2)}$=0.79 which results in 1.73 close protons per tyrosyl. An explanation for this lower value can be found under case 2 in section 4.

A final point concerns the detection of the tyrosine converted into a radical. So far our analysis of time-resolved neutron scattering started from tyr-369 as the most likely radical site. What is the answer from neutron scattering? The answer comes from a test subjecting all the 19 remaining tyrosines as possible radical sites to the same analysis as for tyr-369. The minimum rms values as defined by (6) increase with the distance of the hypothetical radical site from the centre of the catalase molecule [18]. This is true for both sets of input after 1D and 2D Fourier analysis, respectively. Tyr-369 together with tyr-357 and tyr-342 are equally good candidates for a radical site. Tyr-136 with a slightly higher rms deviation might be included as well. TPP selects four tyrosines out of 20 per subunit as possible radical sites (Fig. 7).

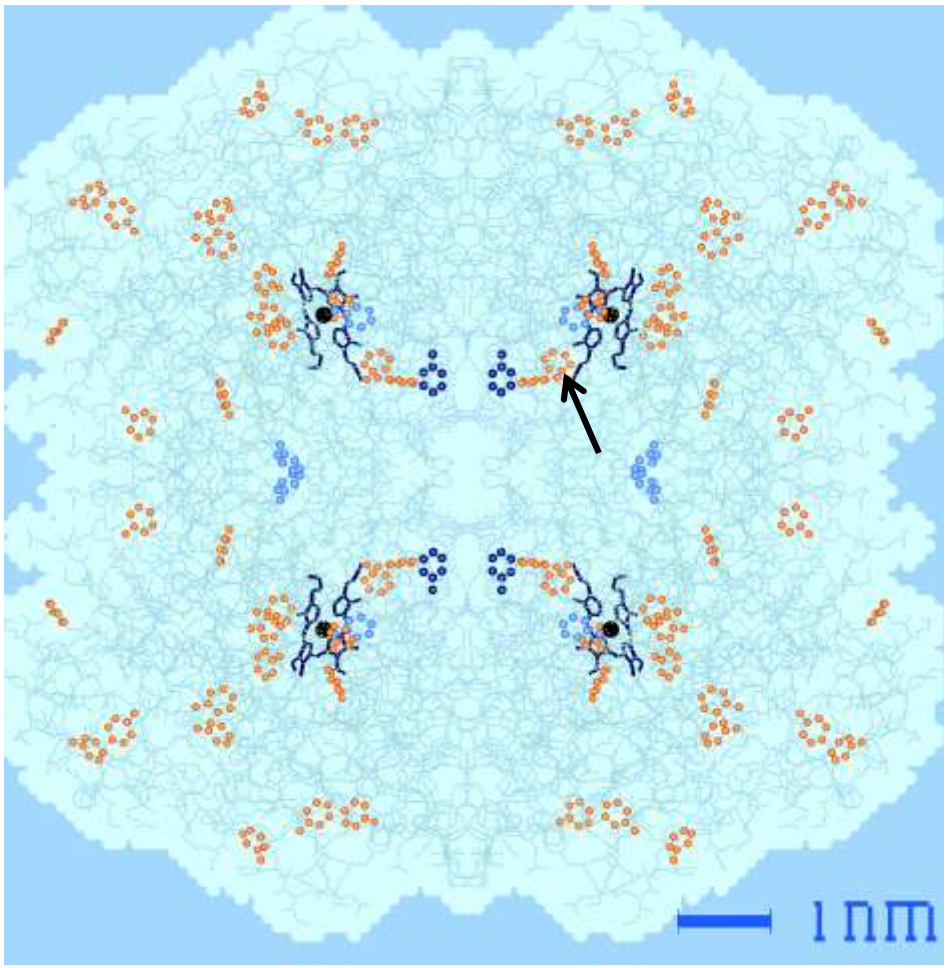

Fig 7. The tetramer bovine liver catalase molecule with its tyrosines presented by their phenyl rings, most of them in orange colour. From neutron scattering it appears that one of the following tyrosines may have become a radical: tyr-324, tyr-357, and tyr-369. They are marked in blue colour. Tyr-136 (marked by an arrow) is another slightly less possible candidate. From EPR [10] tyr-369 is suggested (in dark blue). Tyr-357 is very close to the iron atom (●) of the porphyrin ring [1].

6. Results from time resolved NMR.

The variation of the intensity of proton polarisation during each cycle of DNP has been measured simultaneously with the intensity of neutron scattering. As the sampling of the proton NMR signal takes nearly one second, four points were taken during each half cycle of DNP (Fig. 8). The change of the proton polarisation during one cycle of DNP is largely obscured by electronic noise. Selecting those cycles of DNP supposed to be less contaminated by the noise as described in the Appendix A, we observe a relative change of the proton polarisation close to $\Delta P = 10^{-4}$ which agrees remarkably well with ΔP from time-resolved neutron scattering. Moreover, the Fourier analysed measured proton polarisation follows fairly closely the proton polarisation calculated from the model. We note in passing that the change of the transmission of the catalase sample obtained from $\Delta P = 10^{-4}$ is of the order of 10^{-5}, far below the change of the peak intensities discussed in the preceding section. .

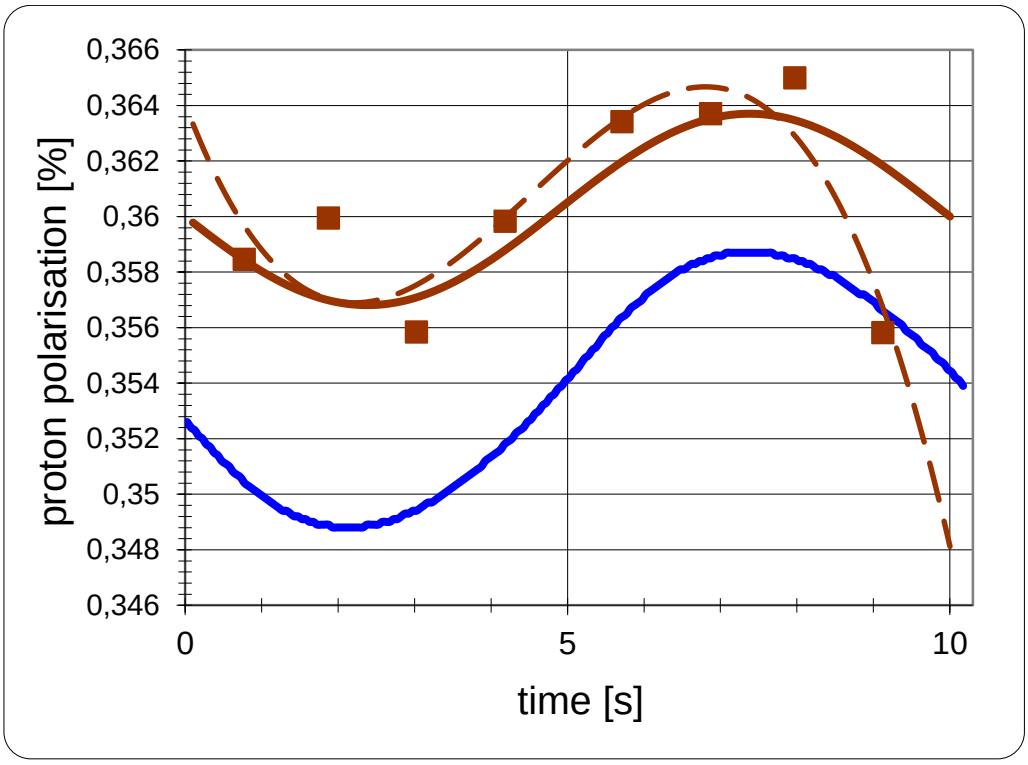

Fig. 8. Comparison of the measured proton polarisation with that obtained from the analysis of time-resolved neutron scattering. ■ measured proton polarisation, ——— its approximation by a Fourier series, and — — — by a polynomial of 3rd degree. ——— proton polarisation obtained from time-resolved neutron scattering. .

7. Outlook.

Two points might be considered in future applications of TPP: A technical one which concerns the optimization of the conditions for DNP. The other, strategic one, which concerns the future use of TPP.

The technical aspect is inspired by Fig. 2, which shows the increase of the proton NMR intensity with DNP at T = 0.1 K and T=1K. In spite of the change of the temperature by an order of magnitude there is nearly no change in the speed of proton polarisation. However the increase of the polarisation comes to an end after half an hour of DNP at T=1K, whereas a continuous increase of polarisation for several hours is observed at T=0.1K. Prolonged irradiation at microwave frequencies below and above the EPR will lead to final values of proton polarisation which become more different at lower temperatures (Fig. 9). An extrapolation to higher temperatures leads to ΔP = 0.01% at T =15 K. What

would be the outcome of time-resolved neutron scattering at T = 10 K? The reservoir R0 then would operate at P_0 = -0.23 and P_0 = +0.23 for negative and positive dynamic polarisation, respectively. The expected change of proton polarisation of 0.015 would be reached within 10 s, approximately. Assuming that nuclear spin diffusion will not depend on the temperature, the method of TPP might still be feasible at higher bath temperatures.

The method of TPP might well find greener pastures in protein crystallography. The determination of the radical density map of proteins then can be achieved in a fairly straight way. The application of the difference Fourier method to time-resolved neutron diffraction allows to follow the evolution of the radical density map in space and time [18]. The change of the intensity of some low–order reflections under the conditions discussed above by 10% looks promising [1].

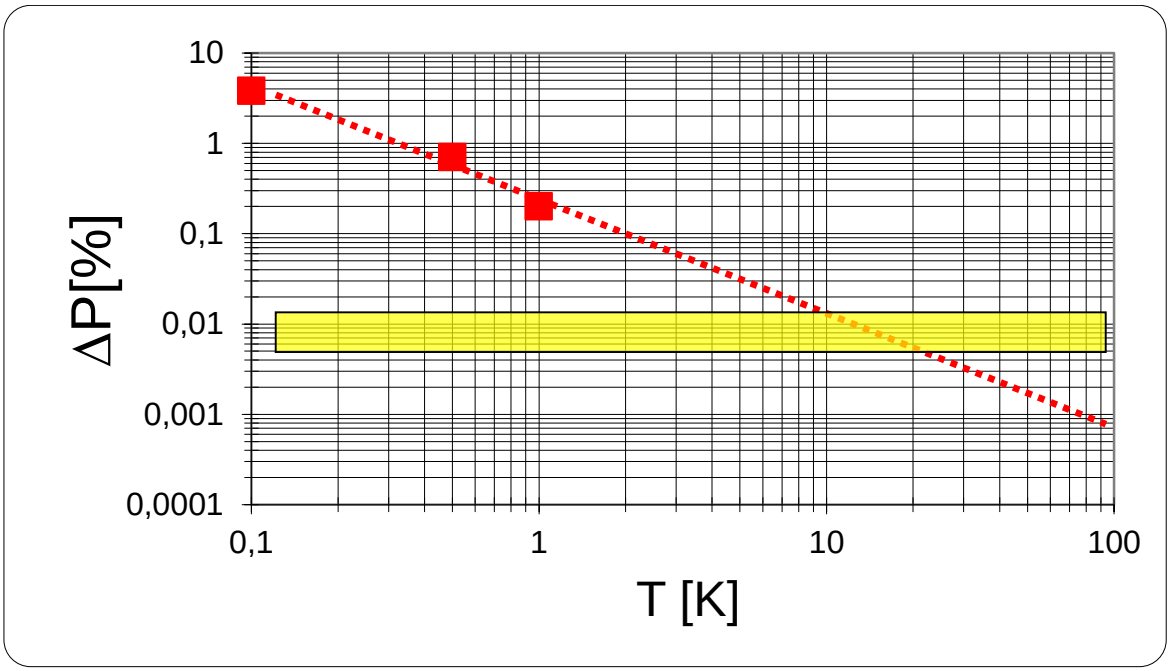

Fig. 9 The difference between the extreme values proton polarisation obtained by positive and negative DNP, respectively, versus the bath temperature. The yellow bar indicates the change of polarisation observed with TPP from catalase at T=0.1 K (this experiment).

8. Acknowledgements

This work was performed by the French-Swiss-German collaboration on the proton polarisation build-up by DNP, the team members of which are B. van den Brandt, H. Glättli, I. Grillo, P. Hautle, J. Kohlbrecher, E. Leymarie, S. Mango, R.P. May, A. Michels, and the authors. We thank the Paul-Scherrer-Institut (PSI) for the use of the facility of dynamic nuclear polarisation, the Institut Laue-Langevin for allocating beam time at the small-angle diffractometer D22, and last not least J. Gaillard (CEN Grenoble) for the EPR measurements. We are grateful to Salvatore Mango with whom we conceived the project at the PSI and to Ben van den Brandt for the successful continuation of the collaboration.

9. Appendix A

The detection of a periodic change of the proton polarisation by $\Delta P \leq 10^{-4}$ during one cycle of DNP is a technical and a numerical challenge. Here we show how the result shown in Fig. 8 has been obtained. The NMR intensity has been measured for 5 hours. At a first glance, there appears to be no periodic change of the NMR intensities with the alternating directions of DNP (Fig. 10). The time frame generator worked correctly. In a next step we calculate the rms of the NMR intensities for each of 1891 cycles of DNP (Fig. 11). A major part of the rms values is a broad band, and a small fraction must be considered

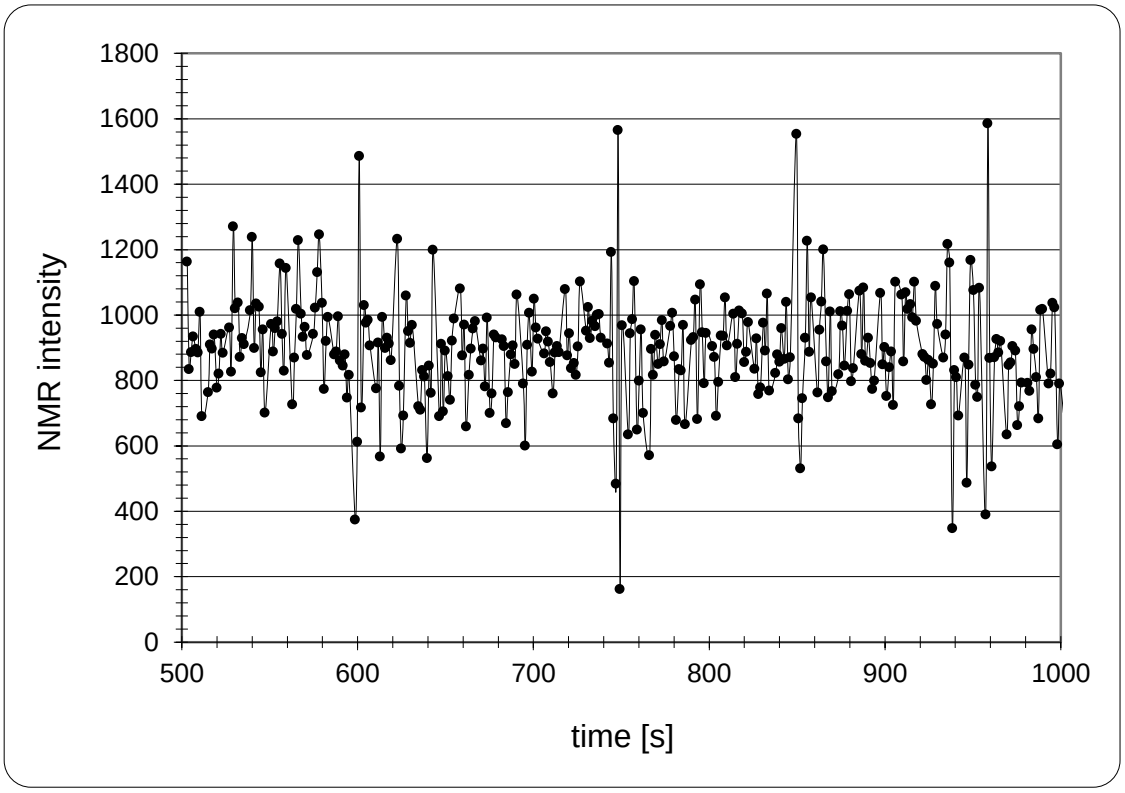

Fig. 10. A part of the NMR data. During one cycle of DNP 8 points were taken. Total time: 5 hours.

as outliers. At this point we cannot exclude 'hidden' outliers inside the majority of cycles represented by their rms values. To test this supposition we subdivide the broad band of rms values into stripes as indicated by the orange bars in Fig. 11. The NMR intensities of each of the 10 subsets are averaged, which results in 8 points for each of the 10 subsets (Fig. 12). The time dependence of NMR has been developed as a Fourier series for each subset. There are large differences among the 10 Fourier representations. We now look for the subsets which present coherent results. They appear to lie in the middle of the 10 subsets: the 3rd, 4th , 5th and 6th are quite similar. We assume that these 4 subsets which comprise the majority of cycles are closest to an unperturbed variation of the NMR intensity during one cycle of DNP.

The NMR intensities reflect proton polarisations close to the thermal equilibrium, i.e. P = 0.35% at B=3.5 T, and T=0.1K. As the NMR intensities are quite small, they are also very sensitive to an off-set due to instrument effects. After inspection of all our NMR data from different samples of catalase it appears that the NMR intensities should be crowded at a value lower than that shown in Fig.12. Using an off-set of 400 we obtain the proton polarisation of the 5th subset shown in Fig. 8 (in brown, both in Fig. 8 and 12).

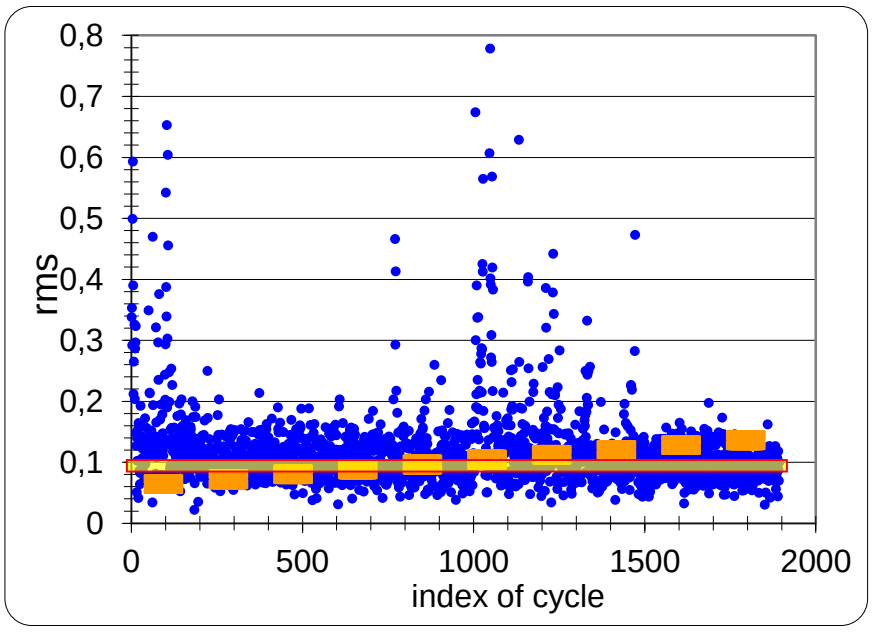

Fig. 11 The rms of the 8 NMR intensities for each cycle of DNP. The orange bars denote limits of intervals of rms. 10 intervals have been chosen. The rms values comprised by the 5th interval (from the left) are within the yellow semi-transparent area, for instance.

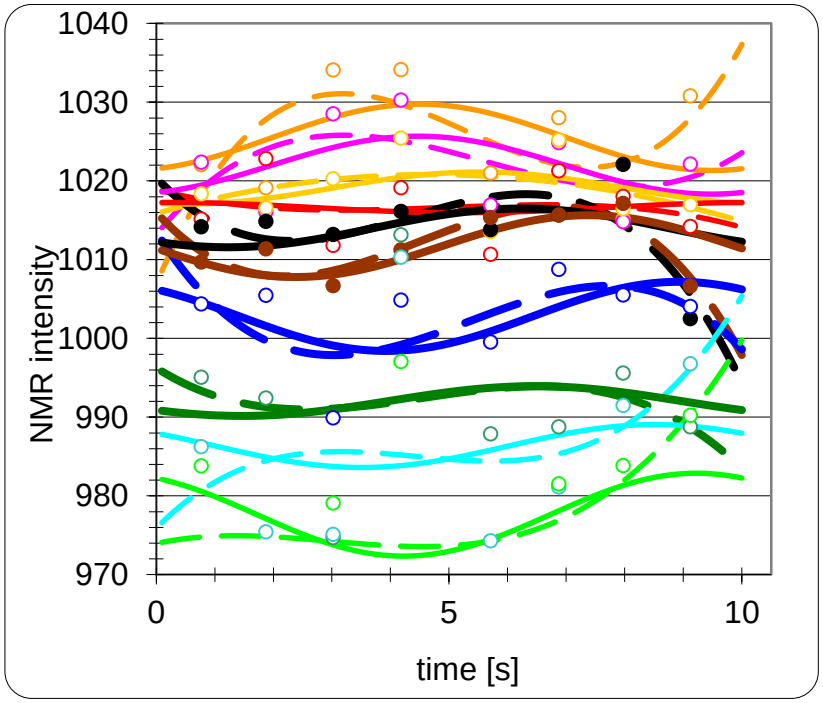

Fig. 12. Time dependent NMR from ten intervals of measured NMR intensities as described in Fig. 11. Interval numbers from lowest to highest intensity. NMR after 1D Fourier analysis: 1, 2, 3, 4, 5, 6, 7, 8, 9, 10. Intervals 5 and 6 are shown in Fig. 13. Broken lines represent a fit by a polynomial of 3rd degree. Symbols are NMR data averaged within a given interval.

References

[1] Zimmer O, Jouve H M, and Stuhrmann H B 2016 IUCrJ, 3, 326-340
[2] Wolfe J P 1973 *Phys. Rev. Lett.* 31 907-910
[3] Bloembergen N (1949 *Physica (Utrecht)* 15 386-426
[4] Furman G B, Goren S D 2002 *Z. Naturforsch.* 57a 307-314
[5] Abragam A, and Goldman M 1978 *Rep. Prog. Phys.* 41 395-468
[6] Abragam A. and Goldman M 1982 *Nuclear Magnetism, Order and Disorder* Oxford University Press
[7] Wenckebach W Th 2016 *Essentials of Dynamic Nuclear Polarisation* Amazon
[8] Cox S F J, Read S F J, and Wenckebach Th 1977 *J. Phys. C: Solid State Phys.* 10 2917-2936
[9] Jannin S, Comment A, and Klink J J 2012 *Applied Magnetic Resonance* 43 59-68
[10] Ivancich A, Jouve H M, Sartor B, and Gaillard J 1997 *Biochemistry* 36 9356-9364
[11] Svistunenko D A, and Cooper C E 2004 *Biophysical J.* 87 582-595
[12] Hayter J B, Jenkin G T, and White J W 1974 *Phys. Rev. Lett.* 33 696-698
[13] Knop W,Nierhaus K H, Novotny V, Niinikoski T O, Krumpolc C, Rieubland J M, Rijllart A, Schärpf O, Schink H-J, Stuhrmann H B and Wagner R 1986 *Helvetica Physica Acta* 50 741-746
[14] Koghi M, Ishida M, Ishikawa Y, Ishimoto S, Kanno Y, Masaike A, Masuda Y, and Morimoto K 1987 *J. Phys. Soc. Japan* 56 2681-2688
[15] Glättli H, Fermon C, Eisenkremer M and Pinot M 1989 *J. Physique* 50 2375-2388
[16] Willumeit R, Burkhardt N, Diedrich G, Zhao J, Nirhaus K H, and Stuhrmann H B (1996) J. Mol. Struct. 383 201-211
[17] Kumada T, Noda Y, Koizumi S, and Hashimoto T 2010 The Journal of Chemical Physics 133 054504
[18] Noda Y, Yamaguchi D, Hashimoto T, Shamoto S, Koizumi S, Yuasa T, Tominaga T and Sone T 2013 *Physica Procedia* 42 52-57
[19] Hautle P, Grübler W, van den Brandt B, Konter J A, Mango S, and Wessler K 1992 *Phys. Rev.* B 46 6596-6599
[20] Buckingham A D 2003 *Chem. Phys. Lett.* 371 517-521
[21] Van den Brandt B, Glättli H, Grillo I, Hautle P, Jouve H, Kohlbrecher J, Konter J A, Leymarie E, Mango S, May R P, Michels A, Stuhrmann H B, and Zimmer O 2004 *Nucl. Instr. and Meth.* A 526 81-90
[22] Van den Brandt b, Glättli H, Grillo I, Hautle P, Jouve H, Kohlbrecher J, Konter J A, Leymarie E, Mango S, May R P, Michel A, Stuhrmann H B and Zimmer O 2006 *Eur. Phys. J.* B 157-165
[23] Stuhrmann H B 2015 *Journal of Optoelectronics and Advanced Materials* 17 1417-1424
[24] Glättli H, and Goldman M 1987 *Methods Exp. Phys.* 23 C 307-314
[25] Fita I, and Rossmann M G 1985 J. Mol. Biol. 185 21-37